Polyethersulfone ultrafiltration membrane modified with polyamic acid-stabilized silver nanoparticles for enhanced filtration performance and antibacterial effects

Kaizhen Wang, Danrong Cai, Die Zou, Ruxue Duan, Wentao Yan, Yong Zhou*, Congjie Gao

Center for Membrane and Water Science & Technology, Zhejiang University of Technology, Hangzhou 310014, China, emails: zhouy@zjut.edu.cn (Y. Zhou), 1441195758@qq.com (K. Wang), 1401764916@qq.com (D. Cai), 1340486550@qq.com (D. Zou), 1831575050@qq.com (R. Duan), yanwentao@zjut.edu.cn (W. Yan), gaocj@zjut.edu.cn (C. Gao)

ABSTRACT

Developing ultrafiltration (UF) membranes with excellent anti-biological fouling and overcoming the hydrophobicity of membrane material itself has been a major challenge. While exposing a major drawback of being unstable and easily lost from the membrane, silver nanoparticles (AgNPs) are still used as bactericidal substances in membranes. Polyamic acid (PAA) is a flexible hydrophilic polymer that exhibits strong complexing ability and considerable steric hindrance effect on metal cations. Herein, using PAA as a stabilizer to modify the size and dispersion of silver nanoparticles (AgNPs), we developed a polyethersulfone (PES) UF membrane featuring both hydrophilic and antibacterial dual functions. The AgNPs in the as-prepared membrane were small in size (around 3–10 nm) and highly dispersed in the membrane, exhibiting highly efficient antibacterial ability with 96.82% and 98.29% inhibition towards *Escherichia coli* and *Staphylococcus aureus*, respectively. Meanwhile, the partially covered AgNPs by PAA and the high surface energy made them less susceptible to lose in the membrane. The developed membrane retained about 4.5 times more AgNPs than the original membrane for the same membrane area. Moreover, the favorable hydrophilic and pore structure endowed the membrane with high water flux and acceptable rejection of bovine serum albumin (BSA). The PES/PAA-Ag membrane exhibited an excellent water flux, which was 421.47 (L/m^2·h) under 1 bar pressure, about 1.4 times of PES and 3.4 times of PES-Ag membrane (with a high BSA rejection, around 90%). This work provided a reference for the development of hydrophilic and antimicrobial membranes, as well as having considerable potential practical value.

Keywords: Ultrafiltration; Polyamic acid; Antibacterial; Silver nanoparticles; Prevent loss

1. Introduction

Almost every substance that enters the environment in nature is subject to the action of one or more microorganisms, whose metabolites or intermediates are complex and diverse, and may accumulate in large quantities under certain conditions, finally causing pollution of the environment or damage to product quality and affecting the service life of product. Membrane separation technology is an emerging and environmentally friendly technology that continues to make breakthroughs in the treatment of water environment, especially in the field of ultrafiltration. Polyethersulfone (PES) is a common raw material for ultrafiltration (UF) membrane preparation. The PES UF membrane is frequently employed in water treatment, chemical, medical and food applications with exceptional

* Corresponding author.

chemical, thermal stability, and mechanical properties [1–5]. However, the conventional PES membranes are susceptible to bacterial adhesion and propagation on the membranes, forming biofilms that can cause irreversible damage to the membrane material. Bacterial fouling severely limits the separation performance and service life of membranes [6–8]. In recent years, the prevalent approach to combat membrane bacterial fouling has been to develop membranes with antibacterial properties [9–11].

The blending of metal nanoparticles with organic polymer membranes to improve the antibacterial properties of membranes has gained recognition [12,13], which potentially inhibits bacterial colonies from forming biofilms on the membrane surface [14]. Modification of membranes with silver nanoparticles (AgNPs) has been shown to be an effective strategy for improving membrane performance and properties [15–17]. Among them, silver nanoparticles (AgNPs) with broad-spectrum bactericidal and fungicidal activities and low toxicity to animal cells have attracted extensive attention [18–21]. Compared with silver ions, AgNPs are persistent and suitable for controlled release [22–24]. Since Chou et al. [25] first reported the antibacterial activity of cellulose acetate-loaded silver, a number of antibacterial membranes loaded with AgNPs have been developed successively. However, there is still a serious problem with AgNPs as bacterial inhibitors in membranes. Because of the weak interaction, AgNPs are not firmly bound to the membrane by physical co-blending and tend to accumulate, which results in a significant loss of antibacterial and antiviral activities [26–30]. According to Khaydarov et al. [31], smaller nanoparticles could enhance the antibacterial and antifungal efficacy. Therefore, it is necessary to focus on the synthesis of AgNPs with small size and high dispersion. The high surface energy and thermodynamic instability of AgNPs lead to their aggregation. Stabilizers are crucial in the fabrication of size-controlled and highly dispersed AgNPs because they effectively stop further AgNP aggregation. Andrade et al. [32] as well as Mukherjee and Bandyopadhyaya [33] fabricated antibacterial membranes of AgNPs using poly(vinylpyrrolidone) and acrylic acid as stabilizers, respectively. However, the size of AgNPs controlled by the above two stabilizers was large (about 40 nm) and easily lost from the membrane. The stable stability of AgNPs in membranes can rely not only on their high surface energy, but also on a polymer with certain properties to hold AgNPs firmly in place. Besides, the large size of AgNPs affects the permeability of membrane. Hence, it is critical to develop membranes that are both antimicrobial and hydrophilic. This requires us not only to consider the antibacterial property and the stability of antibacterial substances in the membrane, as well as improving the permeability of membranes.

Polyamic acid (PAA) has strongly hydrophilic amide and carboxyl groups, as well as chain flexibility [34,35]. The high solubility of PAA in aprotic solvents makes it easy to synthesize and process [36]. It is well known that the compatibility between polymers was a major issue that hinders the performance and stability of membranes. The glass transition temperature (T_g) was a commonly used method to study polymer compatibility [37,38], and the results of our previous study revealed well compatibility

between PES and PAA [39]. Herein, developing a dual-functional PES UF membrane with hydrophilic and antibacterial properties using PAA as a stabilizer to control the size and dispersion of AgNPs. PAA molecules contained a large number of carboxyl groups with strong complexing ability to metal cations and considerable steric hindrance effect. The silver ions were complexed by the carboxyl groups in PAA, and then reduced to highly dispersible and antimicrobial AgNPs by using the reducing property of N,N-dimethylformamide (DMF) solvent. Meanwhile, the chain flexibility of PAA could also partially coat AgNPs and reduce the loss of AgNPs, which effectively extended the antimicrobial life of membranes. Moreover, the hydrophilic group of PAA itself endowed the UF membrane with great hydrophilicity, which could increase the water permeation rate and improve the water flux. Notably, the as-prepared membrane exhibited high water flux at ultra-low pressure. The results of this work indicated that PES UF membrane with hydrophilic and antimicrobial properties prepared by using PAA as a stabilizer was simple and effective, with excellent inhibition of *Escherichia coli* and *Staphylococcus aureus*.

2. Experimental set-up

2.1. Materials

DMF and 4,4'-diaminodiphenyl sulfone (DDS) were supplied by Aladdin Reagent Co., Ltd., (Shanghai, China). Pyromellitic dianhydride (PMDA) was bought from Sinopharm Chemical Reagent Co., Ltd., (Shanghai, China). Bovine serum albumin (BSA, 97%) and silver nitrate (AgNO$_3$, AR) were purchased from Macklin Biochemical Co., Ltd., (Shanghai, China). All chemicals required no further purification.

2.2. Membrane fabrication

All membranes were obtained by NIPS method: PES (15 wt.%), DMF (85 wt.%), and DDS (0.8 g) were mixed in proportion and stirred at 80°C for 0.5 h. PMDA (0.7168 g) and AgNO$_3$ (0.8 g) were added and followed by stirring for 10 h. The casting solution was applied to glass plate and immediately moved to a water bath (20°C) to solidify into a membrane after standing and defoaming for 24 h. Noted as PES/PAA-Ag. Among them, the weight-averaged molecular weight (Mw) of PES and PAA involved were 144,203 and 393,087, and the polydispersity index (PDI) were 1.62 and 2.03, respectively (Fig. S1 and Table S1). Fig. 1 depicted the membrane preparation process as well as a possible mechanism for AgNP formation: DDS and PMDA were poly-condensed to PAA first, and then the silver ions were complexed with carboxyl groups in PAA. Finally, AgNPs were obtained via *in-situ* reduction of silver ions with solvent DMF, coupled with the steric hindrance effect of PAA.

As a control, PES (15 wt.%), DMF (85 wt.%) were blended proportionally and with stirring as long as 0.5 h at 80°C. AgNO$_3$ (0.8 g) was added and solidified to form a membrane after continued stirring for 10 h. Noted as PES-Ag. Similarly, PES (15 wt.%), DMF (85 wt.%) were mixed in proportion and solidified into a membrane after stirring at 80°C
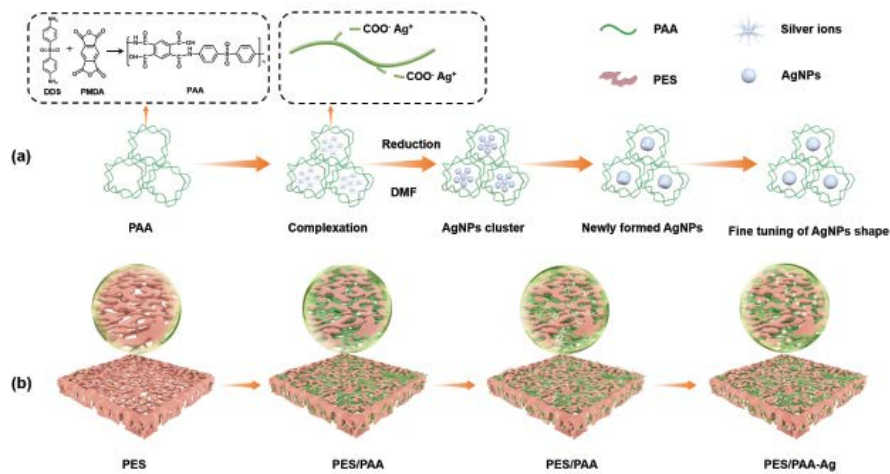
Fig. 1. (a) Diagram of PAA controlled AgNPs size and (b) introduction of AgNPs into PES membrane.

for 10.5 h. Noted as PES. The appearance morphology of the three membranes prepared was shown in Fig. S2.

2.3. Membrane characterization

Transmission electron microscopy (TEM, Hitachi, HT7700 EXALENS, Japan) was used to observe the size and distribution of AgNPs in the membrane. X-ray photoelectron spectroscopy (XPS, Thermo Scientific K-Alpha⁺, America) and Fourier-transform infrared spectroscopy (ATR-FTIR, Nicolet iS50, America) were used for analyzing the chemical composition of membrane surfaces. The membrane morphology structure was studied using atomic force microscopy (AFM, Bruker, Dimension Icon, America) and scanning electron microscopy (SU8010, Hitachi, Japan). The surface roughness of AFM is the ratio of the sample surface area to the scanned area, which is presented as average roughness (R_a) and root-mean-square roughness (R_q), respectively [40]. Identification of AgNPs in PES/PAA-Ag membrane was identified via UV-Vis diffuse reflectance spectroscopy. An X-ray diffractometer (XRD, X'Pert PRO, PANalytical, Netherlands) was used to determine the crystalline structure of AgNPs.

The interfacial free energy of membrane surface ($-\Delta G_{SL}$) can be calculated from Eq. (1) [41]:

$$-\Delta G_{SL} = \gamma_L \left(1 + \cos \frac{\theta}{r} \right) \tag{1}$$

where θ is the average water contact angle (WCA) of membrane surface, γ_L is the liquid's surface tension (surface tension of water at 25°C is 72.8 mJ/m²), and r is the ratio of actual surface area of membrane to planar area.

Through the weight method and Eq. (2) [41], the membrane porosity (ε) was calculated:

$$\varepsilon = \frac{W_w - W_d}{\rho_w \times A \times \delta} \times 100\% \tag{2}$$

where W_w denotes the wet membrane weight, while W_d denotes the dry membrane weight (kg), ρ_w denotes the density of water (0.998 kg/L), A denotes the membrane area (m²), and δ denotes the membrane thickness (m).

2.4. Silver ion release

Prepare 1 cm × 5 cm PES/PAA-Ag and PES-Ag membranes and 15 centrifuge tubes with 8 mL of deionized water. The membranes were immersed in 1 centrifuge tube with deionized water, removed after 24 h and immersed in another centrifuge tube, and then immersed in 15 centrifuge tubes filled with deionized water in sequence. The inductively coupled plasma-optical emission spectrometry (ICP-OES) was employed to test the concentration of silver ions in each centrifuge tube.

2.5. Membrane performance test

Membrane permeability and selectivity were determined via a custom cross-flow filtration system featuring a 7.065 cm² valid membrane cell. The membranes were pre-pressurized at a certain pressure for 0.5 h, and then the water permeation flux was collected and recorded. Next, the membranes selectivity were determined by choosing a 500 ppm BSA solution. Eq. (3) [42] was used to calculate the membrane's water flux (J, L/(m²·h)):

$$J = \frac{\Delta V}{\Delta t \times A} \tag{3}$$

where ΔV refers to the recorded water penetration (L), Δt refers to the filtration time (h), A refers to the effective area (m²).

Using a UV-Vis spectrophotometer (specific wavelength is 278 nm), the BSA concentration was determined. Eq. (4) [42] was used to calculate the BSA retention rate (R):

$$R = \left(1 - \frac{C_p}{C_f} \right) \times 100\% \tag{4}$$

where C_p represents the permeate BSA concentration (g/L), while C_f represents the feed BSA concentration (g/L).

The antibacterial ability of membranes toward *E. coli* and *S. aureus* could be evaluated by the spread plate method. LB broth (10 g/L tryptone, 10 g/L NaCl and 5 g/L yeast powder) was used to make both liquid and solid media for the experiments, which were sterilized by autoclaving. Bacterial suspensions were prepared by incubating the bacteria in a liquid medium for 15 h (37°C, 200 rpm). Afterward, a diluted bacterial suspension (700 μL, 10^6 CFU/mL) was aspirated into a centrifuge tube containing the UV-sterilized membrane (2 cm × 2 cm), making sure to cover the membrane. Then, the membrane was incubated at a constant temperature (37°C) for 6 h. Finally, the culture solution was diluted and spread on the solid culture medium before being incubated for 18 h at 37°C in a constant temperature incubator. Counted colonies and took pictures. The antimicrobial rate (AR) of membrane was calculated using equation (5) [43]:

$$AR = \left(1 - \frac{B}{C}\right) \times 100\% \tag{5}$$

where *B* and *C* are the colony-forming concentrations (CFU/mL) on the control and experimental plates, respectively.

3. Results and discussion

3.1. Membrane properties

IR spectroscopy was utilized to prove the successful incorporation of PAA into the membrane. According to Fig. 2a, the spectrum of PES/PAA-Ag membrane exhibited a new characteristic peak compared to PES membrane.

Specifically, the two peaks at 1,728 and 1,532 cm^{-1} of PES/PAA-Ag membrane were the C=O bond in the carboxyl group and C–N bond in the amide group of PAA, respectively [44,45]. Those results demonstrated that PAA was synthesized and successfully added to the membrane.

To further confirm the above results, the membranes were analyzed using XPS. As depicted in Fig. 2b, PES/PAA-Ag membrane showed a new element at 397.30 eV, while the PES membrane did not. It was most likely the N element of PAA, which provided additional indirect evidence. Furthermore, the characterization of narrow scan spectra was performed. The functional groups C–C/C–H and C–O/C–S were represented by the PES membrane's two major peaks, which were located at 284.8 and 286.2 eV, respectively (Fig. 2c). However, the PES/PAA-Ag membrane did show a new peak (O–C=O/N–C=O) at 288.3 eV (Fig. 2d) [46,47], which was derived only from the functional groups of PAA. Hence, IR and XPS characterization verified that PAA was successfully incorporated into the membrane.

The presence of AgNPs could be determined using UV-Vis diffuse reflectance spectroscopy. As shown in Fig. 3a, there was an absorption peak at 442 nm, indicating the formation of AgNPs. Therefore, it could be concluded that the AgNPs were successfully reduced and incorporated into the PES/PAA-Ag membrane. In contrast, the presence of an absorption peak at 425 nm was indicative of the presence of AgNPs in the PES-Ag membrane. The difference in the location of the absorption peaks of both PES/PAA-Ag and PES-Ag membranes might be related to the variation in the morphology and size of AgNPs formed by the different methods [32]. Moreover, the crystal structure of PAA-stabilized AgNPs was evaluated by XRD. According to
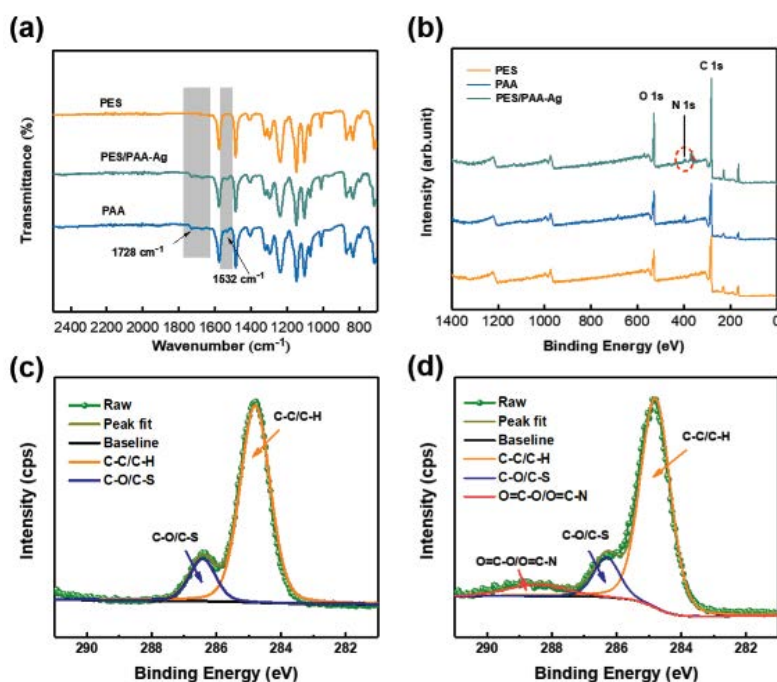
Fig. 2. (a) Fourier-transform infrared spectrum of membrane. (b) X-ray photoelectron spectroscopy wide scan spectrum of membrane. C1 X-ray photoelectron spectroscopy scan spectrum in (c) PES and (d) PES/PAA-Ag membranes.
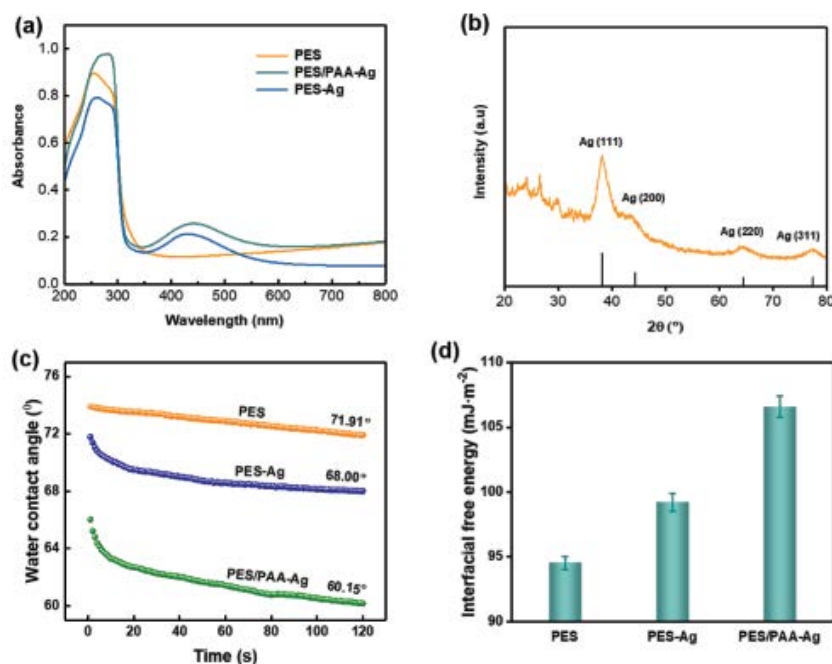
Fig. 3. (a) UV-Vis diffuse reflectance spectrograms of membranes, (b) X-ray diffraction pattern of PAA stabilized silver nanoparticles, (c) dynamic water contact angle of membrane and (d) interfacial free energy of membranes.

Figs. 3b and S3, the diffraction peaks $2\theta = 28.1$, 44.3, 64.4 and 77.4 matched the (111), (200), (220) and (311) crystal planes of face-centered cubic silver phase, respectively [48,49]. This was a typical diffraction pattern of metallic silver, indicating that AgNPs in the PES/PAA-Ag membrane was a face-centred cubic crystal structure. The hydrophilicity of membranes could be characterized by WCA. As shown in Fig. 3c, the WCA of PES/PAA-Ag membrane was lower than PES and PES-Ag, which was 60.2°, implying that the introduced PAA enhanced membrane hydrophilicity. Compared with original WCA, $-\Delta G_{SL}$ could be more representative of the hydrophilicity of membrane [50,51]. In general, the larger the $-\Delta G_{SL}$, the higher the hydrophilicity [52]. It can be seen from Fig. 3d, the $-\Delta G_{SL}$ of PES/PAA-Ag membrane was larger, indicating greater hydrophilicity.

3.2. Morphological structure of membrane

According to Fig. 4a–f, after the control of PAA, the AgNPs in PES/PAA-Ag membrane were generally spherical in shape (particle size around 3–10 nm) and uniformly dispersed in the membrane (Fig. 4e). In contrast, the AgNPs in PES-Ag membrane without PAA as stabilizer showed different morphologies (Fig. 4c), varied sizes and tended to agglomerate into clusters (particle size around 10–150 nm). This phenomenon could also be observed from the back side of membrane (Fig. S4). In addition, AgNPs were observed to be sparsely present in the cross-section of the PES-Ag membrane from TEM images and aggregation of AgNPs could be observed at the top of the membrane (Fig. 4g). However, the difference was that for PES/PAA-Ag membrane, AgNPs were more uniformly dispersed in the cross-section and there was no agglomeration (Fig. 4h). This clearly indicated that PAA as a stabilizer

could control the size of AgNPs and make them uniformly dispersed in the membrane, which was critical for the antibacterial effects. In addition, the roughness and porosity of membranes changed accordingly. The introduction of PAA and AgNPs resulted in a higher roughness of PES/PAA-Ag membrane than PES and PES-Ag membranes (Fig. 4i and Table 1). The reason for the increase of PES/PAA-Ag membrane roughness was that the hydrophilic PAA tended to segregate towards the membrane surface during the phase inversion and the existence of AgNPs on the membrane surface. For the increase of PES-Ag membrane roughness, which was only caused by the AgNPs on the surface. From the roughness presented by the AFM in previous study [39], it could be inferred that the more PAA was introduced and the greater the roughness, the more AgNPs were loaded, which facilitated the antibacterial effects and effectively improved the membrane fouling. In terms of porosity, PES-Ag membrane was reduced by half compared with PES membrane. The reason might be that the pore size formation of membrane was mainly influenced by the solvent and non-solvent exchange rate and the viscosity of casting solution [53]. The hydrophilicity of AgNPs was indeed beneficial to increase the exchange rate of solvent and non-solvent during the phase inversion. Meanwhile, the introduction of AgNPs increased the viscosity of casting solution, which would limit the increase of pore size and porosity of membrane. The WCA results showed that PES-Ag membrane was stronger than PES membrane, but the difference was not significant, indicating that the effect of PES-Ag membrane on the formation of pore size was probably small relative to the viscosity. In addition, the pore size of PES-Ag membrane was likely to be blocked by large AgNPs or aggregated AgNPs clumps, resulting in the decrease of pore size and porosity.
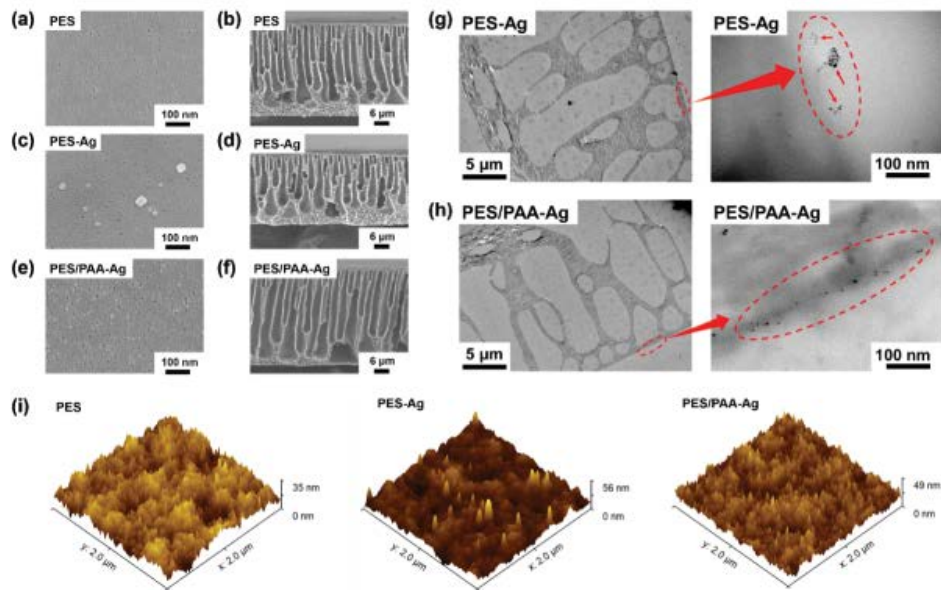
Fig. 4. (a–f) Scanning electron microscopy morphology of membranes, (g–h) Transmission electron microscopy morphology of membranes, and (i) Atomic force microscopy morphology of membranes.

Table 1
Roughness and porosity of the membranes

Membrane	Roughness (nm)		Porosity (%)
	R_a	R_q	
PES	5.14	6.54	35.07 ± 1.31
PES-Ag	6.75	8.38	17.74 ± 2.05
PES/PAA-Ag	7.36	9.09	75.78 ± 1.87

However, for the PES/PAA-Ag membrane, the hydrophilic PAA promoted rapidly fast transfer between solvent-nonsolvent during phase inversion, resulting in membrane with more than twice the porosity of PES membrane.

3.3. Release of silver ions

The immersion technique was used to investigate the static release of AgNPs from PES/PAA-Ag and PES-Ag UF membranes [54]. From Fig. 5a it can be seen that PES/PAA-Ag released more silver ions in the same membrane area, about 4.5 as much as PES-Ag membrane, which indicated that PAA as a stabilizer could effectively prevent the loss of AgNPs and make more AgNPs immobilized and retained on the membrane. One reason was the surface effect of AgNPs. The small-sized AgNPs with high surface energy, a significant percentage of atoms located on the surface, and many dangling bonds were easily adsorbed and loaded on the membrane. Secondly, PAA could achieve partial coating of AgNPs, making AgNPs less likely to be lost (Fig. 5e).

The release of silver ions from membrane was rapid on the first day. The amounts released from PES/PAA-Ag and PES-Ag membranes were 0.1422 and 0.0263 µg/cm^2, respectively (membrane area of 5 cm^2). And then the release of

silver ions gradually stabilized from the next day onwards (Fig. 5b). The reason for this might be the presence of partially superimposed AgNPs, which were weakly bound to the membrane surface and easily dislodged in water, while AgNPs dispersed and immobilized on the membrane surface were more firmly bound to the membrane. Hence, the release of silver ions was faster at first and then gradually slowed down [55]. Meanwhile, as shown in Fig. 5b and c, the amount and rate of daily silver ions released from PES/PAA-Ag membrane were higher than those from PES-Ag since more AgNPs were fixed and retained on PES/PAA-Ag membrane. Also, the small size and high dispersion of AgNPs controlled by PAA as a stabilizer with large specific surface area were more easily oxidized to release silver ions in contact with wate, which was essential for improving the antibacterial performance. As we all know, the World Health Organization (WHO) safety standard for silver ions in drinking water was 100 µg/L, while the maximum release of silver ions through PES/PAA-Ag membrane was 88.89 µg/L, which was lower than the specified standard [56]. In this respect, PES/PAA-Ag membrane might be a potential option for membrane antibacterial disinfection. In addition, for antimicrobial membrane, the longer the antimicrobial capacity, the better the separation performance and service life of membrane. The release of silver ions on membrane was closely related to antimicrobial performance. According to the analysis of Fig. 5d, the total release of silver ions on the membrane for 15 d was 24.91%. Based on the release trend of AgNPs, it was estimated that the antibacterial ability of PES/PAA-Ag membrane could be maintained for at least 60 d, indicating that the membrane exhibited long-lasting antibacterial effects and antimicrobial adsorption ability. Furthermore, the chemical kinetics of AgNPs release reaction was further evaluated (S5). The results revealed that silver ions release exhibited a first-order chemical kinetic model (Fig. S5).

3.4. Antibacterial properties and permeability of membrane

The antibacterial activity of AgNPs was widely documented in the literature, but their mechanism of action against bacteria was not yet fully revealed [32,57]. However, previous studies had indicated that the antibacterial activities of AgNPs might be the result of attachment of AgNPs to cell wall of bacteria, which interfered with cell permeability and respiratory function, leading to cell wall rupture and cell lysis. Meanwhile, silver ions released by nanosilver could react with sulfhydryl groups (–SH) of enzymatic proteins in cells, disrupting protein transport and metabolism, and resulting in the loss of normal biological functions of bacteria [58,59]. In addition, silver ions might produce

reactive oxidizing substances (ROS) that irreversibly damaged the structure and function of DNA [60,61].

Utilizing PES membrane as a control, the antibacterial efficacy of PES-Ag and PES/PAA-Ag membrane was evaluated. Each membrane sample was tested three times in parallel and the results were averaged (Table S2 for the specific data). *E. coli* and *S. aureus* colonies were clearly visible on the PES-Ag membrane in terms of colony growth (Fig. 6b and e), whereas there were significantly fewer colonies on the PES/PAA-Ag membrane (Fig. 6c and f). This revealed that PES/PAA-Ag membrane showed strong antibacterial properties, with 96.82% and 98.29% inhibition towards *E. coli* and *S. aureus*, respectively. In contrast, PES-Ag membrane was almost non-antibacterial ability towards *E. coli* and
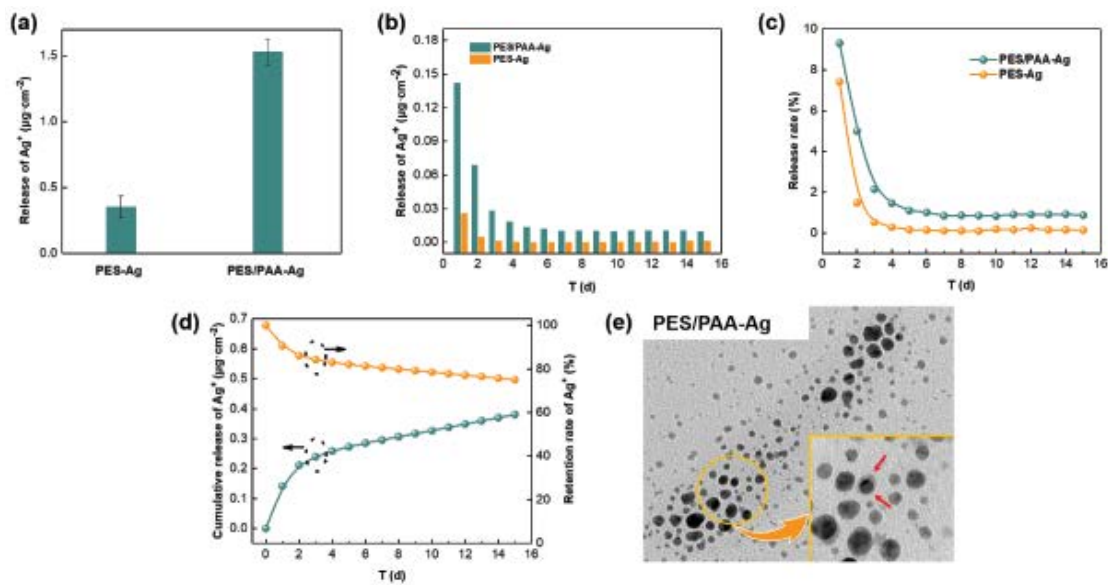
Fig. 5. (a) Total silver ion release from PES/PAA-Ag and PES-Ag membranes of the same area. (b,c) Daily release amount and release rate of silver ions from PES/PAA-Ag and PES-Ag membranes. (d) Cumulative release and retention rate of silver ions on PES/PAA-Ag membrane. (e) Transmission electron microscopy images of AgNPs and PAA (dark black for AgNPs, gray for PAA).
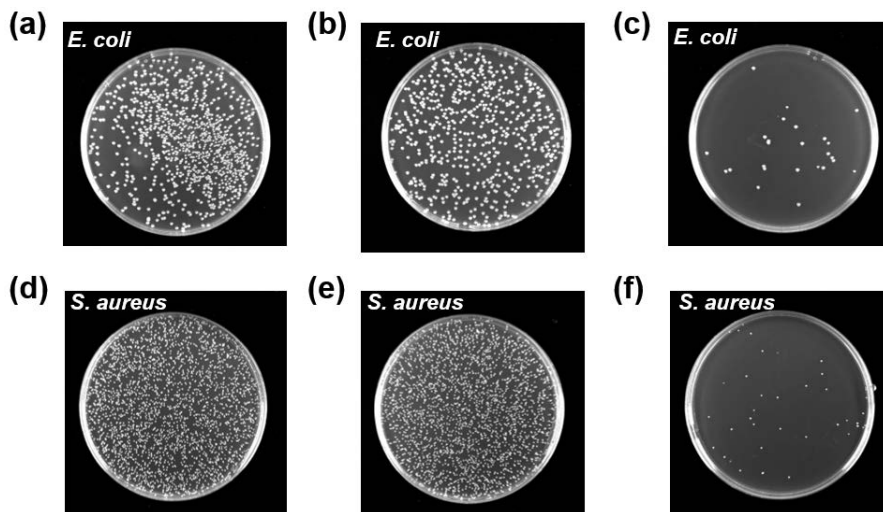
Fig. 6. Colony counts of *Escherichia coli* and *Staphylococcus aureus* on agar plates.
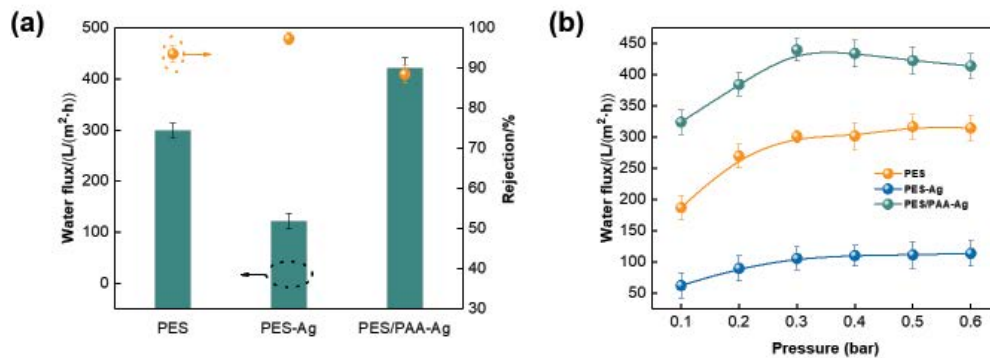
Fig. 7. (a) Membrane water flux and bovine serum albumin rejection at 1 bar pressure and (b) membrane water flux at pressures between 0.1 and 0.6 bar.

only 14.78% inhibition towards *S. aureus*. Small nanoparticles with large surface area were well known to interact more with bacteria and exhibited excellent bactericidal effects [62,63]. AgNPs modified by PAA as stabilizer with small size, large specific surface area and well dispersion, endowed a strong affinity with bacteria. However, AgNPs in PES-Ag membrane without PAA modified were large and easily agglomerated, and the affinity with bacteria was reduced, which seriously affected their antibacterial activity of membrane. Therefore, the PES/PAA-Ag membrane prepared by AgNPs modified with PAA as a stabilizer exhibited excellent antibacterial effects.

As can be seen in Fig. 7a, the water flux of PES/PAA-Ag membrane was higher than that of PES and PES-Ag membranes, which was 421.47 L/m²·h, about 1.4 times of PES and 3.4 times of PES-Ag membrane. One reason was the high hydrophilicity of PAA and AgNPs. On the other hand, the incorporation of PAA increased the thermodynamic instability of casting solution and accelerated the solvent-non-solvent diffusion rate during phase inversion, which caused the surface pore size larger and the porosity increased [53,64,65]. Meanwhile, the BSA rejection of PES/PAA-Ag decreased slightly, while still remaining around 90%. In addition, the morphological analysis of AFM revealed that PES/PAA-Ag displayed the largest roughness (Section 3.2 – Morphological structure of membrane). As we know, the roughness of membrane facilitated the contact between water and membrane, thereby improving the water flux. It could be found that the water flux of PES-Ag membrane was the lowest among three membranes at 121.93 L/m² h, which might be due to the blockage of membrane pores by large-size AgNPs or aggregated AgNPs clusters.

We also tested the water flux at different pressures (0.1–0.6 bar) for the above three membranes (Fig. 7b). The flux of PES/PAA-Ag membrane was above the other two membranes, regardless of the pressure at which they were run. Surprisingly, at 0.3 bar ultra-low pressure, the highest water flux of PES/PAA-Ag membrane could be 440.26 L/m²·h and there was a flux of more than 300 L/m²·h even at 0.1 bar, which was one-tenth of the standard atmospheric pressure. Notably, the flux of PES/PAA-Ag membrane decreased after exceeding 0.3 bar pressure. The reason might be the chain flexibility of PAA, which allowed

Table 2
Antibacterial property of membranes

Type of bacteria	Membrane		
	PES	PES-Ag	PES/PAA-Ag
Escherichia coli	–	–	96.82
Staphylococcus aureus	–	14.78	98.29

the membrane to maintain a great membrane structure under the pressure of 0.3 bar. The structure of membrane might be over-squeezed resulting in the reduction of part of membrane pore channels when the pressure exceeds 0.3 bar, which would lead to a decrease in the water flux of membrane.

4. Conclusions

In this work, we successfully developed a membrane with both hydrophilic and antibacterial properties, that is, PES/PAA-Ag membrane, using PAA as a stabilizer and hydrophilic agent and solvent DMF as a reducing agent. The membrane was given the effective antibacterial ability by the PAA stabilizer because it was able to control the size of AgNPs and display significant dispersion within the membrane. Importantly, the partial coverage of AgNPs by PAA and the high surface energy effectively prevented them from being easily lost in the membrane, and the developed PES/PAA-Ag membrane retained 4.5 times more AgNPs than the PES membrane. Unexpectedly, the hydrophilicity and porosity imparted to the membrane by PAA resulted in a significant improvement in membrane permeability. Meanwhile, the static release of AgNPs resulted in silver ions release through the membrane that was sufficient to meet the WHO standard for silver ions in drinking water. In a word, this study offered a potential way of thinking and application for the development of dual functional membranes with both bacteria removal and high flux.

References

[1] M.T. Tsehaye, S. Velizarov, B. Van der Bruggen, Stability of polyethersulfone membranes to oxidative agents: a review, Polym. Degrad. Stab., 157 (2018) 15–33.

[2] S. Lotfi, K. Fischer, A. Schulze, A.I. Schafer, Photocatalytic degradation of steroid hormone micropollutants by TiO_2-coated polyethersulfone membranes in a continuous flow-through process, Nat. Nanotechnol., 17 (2022) 417–423.

[3] C. Zhao, J. Xue, F. Ran, S. Sun, Modification of polyethersulfone membranes – a review of methods, Prog. Mater Sci., 58 (2013) 76–150.

[4] W. Wang, Y. Kang, C. Cui, X. Lv, Z. Wang, B. Wang, Y. Tan, S. Jiao, G. Pang, Fabrication of under liquid dual superlyophobic membrane via anchoring polyethersulfone nanoparticles on Zn-Ni-Co layered double hydroxide (LDH) nanowires with stainless steel mesh as supporter, Sep. Purif. Technol., 294 (2022) 121148, doi: 10.1016/j.seppur.2022.121148.

[5] M. Ouda, A. Hai, R. Krishnamoorthy, B. Govindan, I. Othman, C.C. Kui, M.Y. Choi, S.W. Hasan, F. Banat, Surface tuned polyethersulfone membrane using an iron oxide functionalized halloysite nanocomposite for enhanced humic acid removal, Environ. Res., 204 (2022) 112113, doi: 10.1016/j.envres.2021.112113.

[6] M. Aslam, R. Ahmad, J. Kim, Recent developments in biofouling control in membrane bioreactors for domestic wastewater treatment, Sep. Purif. Technol., 206 (2018) 297–315.

[7] J. Yang, X. Zhu, J. Lin, Q. Wang, L. Zhang, N. Yang, L. Lin, J. Zhao, Y. Zhao, L. Chen, Integration of a hydrophilic hyperbranched polymer and a quaternary ammonium compound to mitigate membrane biofouling, ACS Appl. Polym. Mater., 4 (2022) 229–239.

[8] L. Ren, J. Chen, Q. Lu, J. Han, H. Wu, Anti-biofouling nanofiltration membrane constructed by *in-situ* photografting bactericidal and hydrophilic polymers, J. Membr. Sci., 617 (2021) 118658, doi: 10.1016/j.memsci.2020.118658.

[9] W. Wang, L. Zhu, B. Shan, C. Xie, C. Liu, F. Cui, G. Li, Preparation and characterization of SLS-CNT/PES ultrafiltration membrane with antifouling and antibacterial properties, J. Membr. Sci., 548 (2018) 459–469.

[10] Z. Qiu, J. Chen, R. Dai, Z. Wang, Modification of ultrafiltration membrane with antibacterial agent intercalated layered nanosheets: toward superior antibiofouling performance for water treatment, Water Res., 219 (2022) 118539, doi: 10.1016/j.watres.2022.118539.

[11] S. Dadari, M. Rahimi, S. Zinadini, Novel antibacterial and antifouling PES nanofiltration membrane incorporated with green synthesized nickel-bentonite nanoparticles for heavy metal ions removal, Chem. Eng. J., 431 (2022) 134116, doi: 10.1016/j.cej.2021.134116.

[12] K. Zodrow, L. Brunet, S. Mahendra, D. Li, A. Zhang, Q. Li, P.J. Alvarez, Polysulfone ultrafiltration membranes impregnated with silver nanoparticles show improved biofouling resistance and virus removal, Water Res., 43 (2009) 715–723.

[13] S. Al Aani, V. Gomez, C.J. Wright, N. Hilal, Fabrication of antibacterial mixed matrix nanocomposite membranes using hybrid nanostructure of silver coated multi-walled carbon nanotubes, Chem. Eng. J., 326 (2017) 721–736.

[14] A. Avornyo, A. Thanigaivelan, R. Krishnamoorthy, S.W. Hassan, F. Banat, Ag-CuO-decorated ceramic membranes for effective treatment of oily wastewater, Membranes, 13 (2023) 176, doi: 10.3390/membranes13020176.

[15] S. Liu, F. Fang, J. Wu, K. Zhang, The anti-biofouling properties of thin-film composite nanofiltration membranes grafted with biogenic silver nanoparticles, Desalination, 375 (2015) 121–128.

[16] X. Wu, F. Fang, B. Zhang, J.J. Wu, K. Zhang, Biogenic silver nanoparticles-modified forward osmosis membranes with mitigated internal concentration polarization and enhanced antibacterial properties, npj Clean Water, 5 (2022) 50, doi: 10.1038/s41545-022-00199-6.

[17] S. Liu, M. Zhang, F. Fang, L. Cui, J. Wu, R. Field, K. Zhang, Biogenic silver nanocomposite TFC nanofiltration membrane with antifouling properties, Desal. Water Treat., 57 (2015) 10560–10571.

[18] H. Zhao, M. Wang, Y. Cui, C. Zhang, Can we arrest the evolution of antibiotic resistance? The differences between the effects of silver nanoparticles and silver ions, Environ. Sci. Technol., 56 (2022) 5090–5101.

[19] Z. Liu, Y. Hu, Sustainable antibiofouling properties of thin film composite forward osmosis membrane with rechargeable silver nanoparticles loading, ACS Appl. Mater. Interfaces, 8 (2016) 21666–21673.

[20] S. Chernousova, M. Epple, Silver as antibacterial agent: ion, nanoparticle, and metal, Angew. Chem. Int. Ed. Engl., 52 (2013) 1636–1653.

[21] B. Le Ouay, F. Stellacci, Antibacterial activity of silver nanoparticles: a surface science insight, Nano Today, 10 (2015) 339–354.

[22] Y. Lv, H. Liu, Z. Wang, S. Liu, L. Hao, Y. Sang, D. Liu, J. Wang, R.I. Boughton, Silver nanoparticle-decorated porous ceramic composite for water treatment, J. Membr. Sci., 331 (2009) 50–56.

[23] X. Li, R. Pang, J. Li, X. Sun, J. Shen, W. Han, L. Wang, *In-situ* formation of Ag nanoparticles in PVDF ultrafiltration membrane to mitigate organic and bacterial fouling, Desalination, 324 (2013) 48–56.

[24] D.Y. Zhang, Q. Hao, J. Liu, Y.S. Shi, J. Zhu, L. Su, Y. Wang, Antifouling polyimide membrane with grafted silver nanoparticles and zwitterion, Sep. Purif. Technol., 192 (2018) 230–239.

[25] W. Chou, D. Yu, M. Yang, The preparation and characterization of silver-loading cellulose acetate hollow fiber membrane for water treatment, Polym. Adv. Technol., 16 (2005) 600–607.

[26] S. Qin, M. Xie, S. Cao, J. Li, L. Wang, S.H. Luo, M. Lv, Insight into the antibacterial resistance of graphdiyne functionalized by silver nanoparticles, Cell Proliferation, 55 (2022) e13236, doi: 10.1111/cpr.13236.

[27] P. Wang, H. Zhu, S. Bao, M. Du, M. Zhang, AgNPs/PVA and AgNPs/(PVA/PEI) hybrids: preparation, morphology and antibacterial activity, J. Phys. D: Appl. Phys., 46 (2013) 345303, doi: 10.1088/0022-3727/46/34/345303.

[28] X. Dai, Q. Guo, Y. Zhao, P. Zhang, T. Zhang, X. Zhang, C. Li, Functional silver nanoparticle as a benign antimicrobial agent that eradicates antibiotic-resistant bacteria and promotes wound healing, ACS Appl. Mater. Interfaces, 8 (2016) 25798–25807.

[29] W. Shao, X. Liu, H. Min, G. Dong, Q. Feng, S. Zuo, Preparation, characterization, and antibacterial activity of silver nanoparticle-decorated graphene oxide nanocomposite, ACS Appl. Mater. Interfaces, 7 (2015) 6966–6973.

[30] Y. Zhou, J. Yang, T. He, H. Shi, X. Cheng, Y. Lu, Highly stable and dispersive silver nanoparticle-graphene composites by a simple and low-energy-consuming approach and their antimicrobial activity, Small, 9 (2013) 3445–3454.

[31] R.R. Khaydarov, R.A. Khaydarov, Y. Estrin, S. Evgrafova, T. Scheper, C. Endres, S.Y. Cho, Nanomaterials: Risks and Benefits, I. Linkov, J. Steevens, Eds., Springer, Dordrecht, 2009, pp. 287–297.

[32] P.F. Andrade, A.F. de Faria, S.R. Oliveira, M.A. Arruda, C. Goncalves Mdo, Improved antibacterial activity of nanofiltration polysulfone membranes modified with silver nanoparticles, Water Res., 81 (2015) 333–342.

[33] M. Mukherjee, R. Bandyopadhyaya, Silver nanoparticle impregnated polyethersulfone ultrafiltration membrane: optimization of degree of grafting of acrylic acid for biofouling prevention and improved water permeability, J. Environ. Chem. Eng., 8 (2020) 103711, doi: 10.1016/j.jece.2020.103711.

[34] E. Zhang, Y. Zhao, W. Yang, H. Chen, W. Liu, X. Dai, X. Qiu, X. Ji, Viscoelastic behaviour and relaxation modes of one polyamic acid organogel studied by rheometers and dynamic light scattering, Soft Matter, 14 (2017) 73–82.

[35] H.C. Yu, J.Y. Choi, J.W. Jeong, B.J. Kim, C.M. Chung, Simple and easy recycling of poly(amic acid) gels through microwave irradiation, J. Polym. Sci., Part A: Polym. Chem., 55 (2017) 981–987.

[36] S. Hamnca, J. Chamier, S. Grant, T. Glass, E. Iwuoha, P. Baker, Spectroscopy, morphology, and electrochemistry of electrospun polyamic acid nanofibers, Front. Chem., 9 (2021) 782813, doi: 10.3389/fchem.2021.782813.

[37] D. Rana, K. Bag, S.N. Bhattacharyya, B.M. Mandal, Miscibility and phase diagrams of poly(phenyl acrylate) and poly(styrene-co-acrylonitrile) blends, J. Polym. Sci., Part B: Polym. Phys., 38 (2000) 369–375.

[38] D. Rana, B.M. Mandal, S.N. Bhattacharyya, Miscibility of poly(styrene-co-butyl acrylate) with poly(ethyl methacrylate): existence of both UCST and LCST, Polym. Plast. Technol. Eng., 34 (1993) 1454–1459.

[39] K. Wang, S. Wang, K. Gu, W. Yan, Y. Zhou, C. Gao, Ultra-low pressure PES ultrafiltration membrane with high-flux and enhanced anti-oil-fouling properties prepared via *in-situ* polycondensation of polyamic acid, Sci. Total Environ., 842 (2022) 156661, doi: 10.1016/j.scitotenv.2022.156661.

[40] K. Rambabu, S. Gokul, A.S. Russel, A. Sivaramakrishna, B. Ponnusami, F. Banat, Lithium perchlorate modified nanoporous polyethersulfone membranes for improved dye rejection, Desal. Water Treat., 122 (2018) 146–157.

[41] T. Arumugham, M. Ouda, R. Krishnamoorthy, A. Hai, N. Gnanasundaram, S.W. Hasan, F. Banat, Surface-engineered polyethersulfone membranes with inherent Fe-Mn bimetallic oxides for improved permeability and antifouling capability, Environ. Res., 204 (2022) 112390, doi: 10.1016/j.envres.2021.112390.

[42] P. Kallem, G. Bharath, K. Rambabu, C. Srinivasakannan, F. Banat, Improved permeability and antifouling performance of polyethersulfone ultrafiltration membranes tailored by hydroxyapatite/boron nitride nanocomposites, Chemosphere, 268 (2021) 129306, doi: 10.1016/j.chemosphere.2020.129306.

[43] D. Coelho, A. Sampaio, C. Silva, H.P. Felgueiras, M.T.P. Amorim, A. Zille, Antibacterial electrospun poly(vinyl alcohol)/enzymatic synthesized poly(catechol) nanofibrous midlayer membrane for ultrafiltration, ACS Appl. Mater. Interfaces, 9 (2017) 33107–33118.

[44] Y. Zhai, Q. Yang, R. Zhu, Y. Gu, The study on imidization degree of polyamic acid in solution and ordering degree of its polyimide film, J. Mater. Sci., 43 (2007) 338–344.

[45] K.H. Moon, B. Chae, K.S. Kim, S.W. Lee, Y.M. Jung, Preparation and characterization of transparent polyimide-silica composite films using polyimide with carboxylic acid groups, Polymers, 11 (2019) 1–10.

[46] D.T. Padavan, W.K. Wan, Synthesis and characterization of a novel versatile poly(amic acid) derived from ethylenediaminetetraacetic dianhydride, Mater. Chem. Phys., 124 (2010) 427–433.

[47] Z. Wang, Z. Wu, Y. Zhang, J. Meng, Hyperbranched-polyol-tethered poly(amic acid) electrospun nanofiber membrane with ultrahigh adsorption capacity for boron removal, Appl. Surf. Sci., 402 (2017) 21–30.

[48] S.M. Imran, S.A. Moiz, M.M. Ahmed, J.H. Lee, H.T. Kim, Structural Characterization of the Silver-Polyaniline Nanocomposite for Electronic Devices, 2009 IEEE 13th International Multitopic Conference, IEEE, Islamabad, Pakistan, 2009, pp. 1–4.

[49] M.S. Haider, G.N. Shao, S.M. Imran, S.S. Park, N. Abbas, M.S. Tahir, M. Hussain, W. Bae, H.T. Kim, Aminated polyethersulfone-silver nanoparticles (AgNPs-APES) composite membranes with controlled silver ion release for antibacterial and water treatment applications, Mater. Sci. Eng., C, 62 (2016) 732–745.

[50] A.K. Ghosh, B.H. Jeong, X. Huang, E.M.V. Hoek, Impacts of reaction and curing conditions on polyamide composite reverse osmosis membrane properties, J. Membr. Sci., 311 (2008) 34–45.

[51] G. Hurwitz, G.R. Guillen, E.M.V. Hoek, Probing polyamide membrane surface charge, zeta potential, wettability, and hydrophilicity with contact angle measurements, J. Membr. Sci., 349 (2010) 349–357.

[52] Y. Chen, R. Sun, W. Yan, M. Wu, Y. Zhou, C. Gao, Antibacterial polyvinyl alcohol nanofiltration membrane incorporated with $Cu(OH)_2$ nanowires for dye/salt wastewater treatment, Sci. Total Environ., 817 (2022) 152897, doi: 10.1016/j.scitotenv.2021.152897.

[53] M. Sadrzadeh, S. Bhattacharjee, Rational design of phase inversion membranes by tailoring thermodynamics and kinetics of casting solution using polymer additives, J. Membr. Sci., 441 (2013) 31–44.

[54] M. Zhang, K. Zhang, B. De Gusseme, W. Verstraete, Biogenic silver nanoparticles (bio-Ag^0) decrease biofouling of bio-Ag^0/PES nanocomposite membranes, Water Res., 46 (2012) 2077–2087.

[55] X. Cao, M. Tang, F. Liu, Y. Nie, C. Zhao, Immobilization of silver nanoparticles onto sulfonated polyethersulfone membranes as antibacterial materials, Colloids Surf., B, 81 (2010) 555–562.

[56] M. Zhang, R.W. Field, K. Zhang, Biogenic silver nanocomposite polyethersulfone UF membranes with antifouling properties, J. Membr. Sci., 471 (2014) 274–284.

[57] W.K. Jung, H.C. Koo, K.W. Kim, S. Shin, S.H. Kim, Y.H. Park, Antibacterial activity and mechanism of action of the silver ion in *Staphylococcus aureus* and *Escherichia coli*, Appl. Environ. Microbiol., 74 (2008) 2171–2178.

[58] I. Sondi, B. Salopek-Sondi, Silver nanoparticles as antimicrobial agent: a case study on *E. coli* as a model for gram-negative bacteria, J. Colloid Interface Sci., 275 (2004) 177–182.

[59] J.A. Lemire, J.J. Harrison, R.J. Turner, Antimicrobial activity of metals: mechanisms, molecular targets and applications, Nat. Rev. Microbiol., 11 (2013) 371–384.

[60] Z. Xu, S. Ye, G. Zhang, W. Li, C. Gao, C. Shen, Q. Meng, Antimicrobial polysulfone blended ultrafiltration membranes prepared with Ag/Cu_2O hybrid nanowires, J. Membr. Sci., 509 (2016) 83–93.

[61] P.V. AshaRani, G.L.K. Mun, M.P. Hande, S. Valiyaveettil, Cytotoxicity and genotoxicity of silver nanoparticles in human cells, ACS Nano, 3 (2008) 279–290.

[62] B. Ajitha, Y. Ashok Kumar Reddy, P. Sreedhara Reddy, Enhanced antimicrobial activity of silver nanoparticles with controlled particle size by pH variation, Powder Technol., 269 (2015) 110–117.

[63] C. Baker, A. Pradhan, L. Pakstis, D.J. Pochan, S.I. Shah, Synthesis and antibacterial properties of silver nanoparticles, J. Nanosci. Nanotechnol., 5 (2005) 244–249.

[64] Q. Zheng, P. Wang, Y. Yang, D. Cui, The relationship between porosity and kinetics parameter of membrane formation in PSF ultrafiltration membrane, J. Membr. Sci., 286 (2006) 7–11.

[65] G.R. Guillen, Y. Pan, M. Li, E.M.V. Hoek, Preparation and characterization of membranes formed by nonsolvent induced phase separation: a review, Ind. Eng. Chem. Res., 50 (2011) 3798–3817.

Supporting information

S5. Determination of chemical kinetics of silver (Ag+) ion release from PES/PAA-Ag membrane
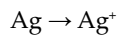
$$Ag \rightarrow Ag^+$$

Rate of reaction:

$$Rate = -\frac{\Delta[Ag]}{\Delta t} = -k[Ag]$$

Assuming the first-order kinetic model to be valid:

$$\frac{-d[Ag]}{dt} = -k[Ag]$$

Rearranging variables:

$$\frac{d[Ag]}{[Ag]} = kdt \tag{S5.1}$$
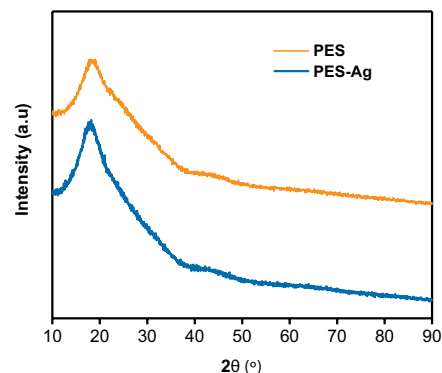
Fig. S3. X-ray diffraction pattern of PES and PES-Ag membranes. Pure PES membrane exhibited a broad peak in the 18° 2θ range, which corresponds to an amorphous structure.

Table S1
Molecular weight and polydispersity index of polymers

Name	Mn	Mw	PDI
PES	89,211	144,203	1.62
PAA	193,484	393,087	2.03
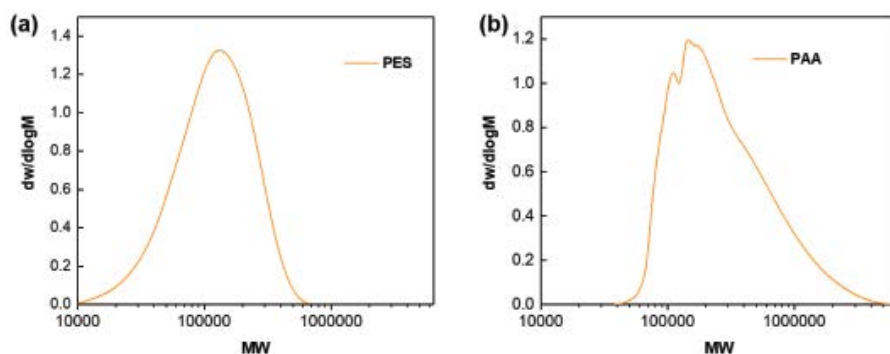
Fig. S1. Molecular weight distribution curve of PES and PAA.
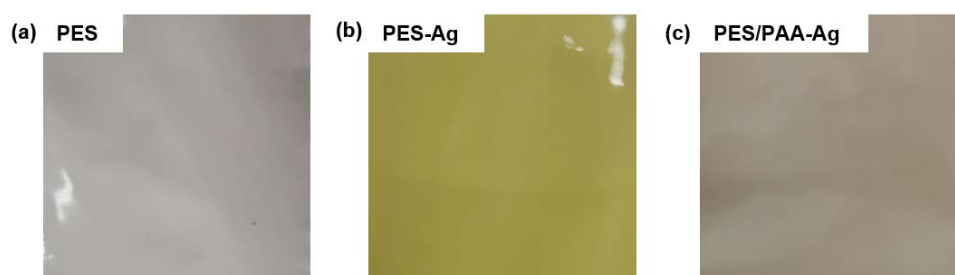
Fig. S2. Appearance of membranes. PES membrane is white, PES-Ag and PES/PAA-Ag are yellow and light brown, respectively.
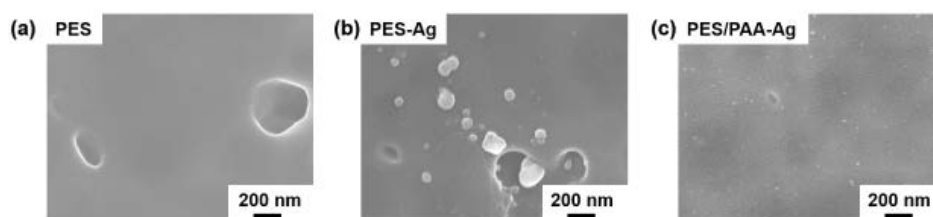
Fig. S4. Backside of PES, PES-Ag and PES/PAA-Ag membranes.

Integrating the Eq. (S5.1) to obtain linearized integral form:

$$\int_{Ag}^{Ag^+} \frac{d[Ag]}{[Ag]} = k\int_0^t dt$$

$$\ln[Ag^+] - \ln[Ag] = kt$$

$$\ln[Ag^+] = kt + \ln[Ag] \tag{S5.2}$$

Using Eq. (S5.2) to plot graph between ln[Ag$^+$] and time.

$$y = mx + b$$

Further, the linear regression of the plot (Fig. S5) between logarithm values of Ag$^+$ ions concentrations and time was

obtained. The coefficient of determination (R^2) 0.94, illustrates that the silver ion release shows excellent fit to first-order kinetic model.
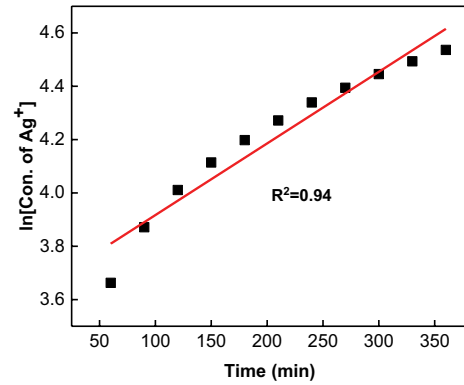
Fig. S5. First-order chemical kinetic model for Ag$^+$ ion released from PES/PAA-Ag membrane.

Table S2
Concentration of membrane bacteria after culture

Membrane	Concentration of *Escherichia coli* (CFU/mL)			Concentration of *Staphylococcus aureus* (CFU/mL)		
PES	1.23×10^9	9.10×10^8	1.24×10^9	3.20×10^9	1.13×10^9	2.91×10^9
PES-Ag	1.23×10^9	1.36×10^9	1.28×10^9	2.28×10^9	1.29×10^9	2.60×10^9
PES/PAA-Ag	3.80×10^7	2.63×10^7	4.30×10^7	4.30×10^7	3.58×10^7	4.50×10^7